Erschienen in: Nature ; 600 (2021), 7890. - S. 754-758
https://doi.org/10.1038/s41586-021-04214-7

β-NAD as a building block in natural product biosynthesis

Lena Barra[1,4], Takayoshi Awakawa[1,2,4]✉, Kohei Shirai[1], Zhijuan Hu[1], Ghader Bashiri[3] & Ikuro Abe[1,2]✉

β-Nicotinamide adenine dinucleotide (β-NAD) is a pivotal metabolite for all living organisms and functions as a diffusible electron acceptor and carrier in the catabolic arms of metabolism[1,2]. Furthermore, β-NAD is involved in diverse epigenetic, immunological and stress-associated processes, where it is known to be sacrificially utilized as an ADP-ribosyl donor for protein and DNA modifications, or the generation of cell-signalling molecules[3,4]. Here we report the function of β-NAD in secondary metabolite biosynthetic pathways, in which the nicotinamide dinucleotide framework is heavily decorated and serves as a building block for the assembly of a novel class of natural products. The gatekeeping enzyme of the discovered pathway (SbzP) catalyses a pyridoxal phosphate-dependent [3+2]-annulation reaction between β-NAD and *S*-adenosylmethionine, generating a 6-azatetrahydroindane scaffold. Members of this novel family of β-NAD-tailoring enzymes are widely distributed in the bacterial kingdom and are encoded in diverse biosynthetic gene clusters. The findings of this work set the stage for the discovery and exploitation of β-NAD-derived natural products.

Natural products are of tremendous importance for human health purposes as they are either directly utilized as potent medicinal drugs or provide valuable structural leads for drug development[5]. They are typically classified according to their primary metabolite biosynthetic origin and the specialized enzyme families responsible for their assembly[6]. Biosynthetically well-established natural product classes, such as terpenoids, polyketides or non-ribosomal peptides, are derived from oligoprenyl diphosphates, activated C2-building blocks such as malonyl-CoA, or amino acids, respectively, and their carbon scaffolds are assembled by terpene synthases, polyketide synthases and non-ribosomal peptide synthetases, so-called core biosynthetic enzymes[6,7]. The anticancer compound altemicidin (**1**), as well as the Ile-tRNA synthetase inhibitors SB-203207 (**2**) and SB-203208 (**3**) are structurally highly unusual natural products, exhibiting a unique 6-azatetrahydroindane scaffold[8–11] (Fig. 1a). Resistance gene-guided genome mining[12] recently enabled us to identify the biosynthetic gene cluster (*sbz* cluster; Supplementary Table 1) for **1**–**3** in the producer strain *Streptomyces* sp. NCIMB40513, and initial studies revealed the enzymatic basis for the scaffold tailoring steps, namely, the installation of the sulfamoylacetic acid and β-methylphenylalanine side chains[13] (Supplementary Fig. 1). The seven remaining, functionally uncharacterized gene products in the *sbz* cluster (Fig. 1b) did not exhibit significant homology to typical core biosynthetic enzymes from known natural product biosynthetic pathways, raising the question of how nature assembles the unusual 6-azatetrahydroindane scaffold.

Identification of the gatekeeping enzyme SbzP

Taking into account that one of the seven remaining gene products (Fig. 1b) would catalyse the formation of the first committed pathway intermediate by utilizing specific building blocks from the primary metabolite pool, each gene was separately expressed in a heterologous host (*Streptomyces lividans* TK21) and culture extracts were subjected to an untargeted metabolomics analysis.

As a result, a specific metabolite was detected in the *sbzP* expression strain and the structure was determined as nucleoside **4** (Fig. 1c), exhibiting the characteristic 6-azatetrahydroindane scaffold of **1**–**3**, but differing in terms of an additional unsaturation in the tetrahydropyridine ring and an *N*-ribosyl linkage. Furthermore, trace amounts of a monophosphate analogue (**4b**) were detected in the high-polarity region (Fig. 1c). These findings demonstrated that the pyridoxal phosphate (PLP)-dependent protein SbzP acts as the gatekeeping enzyme of the *sbz* pathway and is solely responsible for the formation of the 6-azatetrahydroindane scaffold, as well as an unexpected nucleotide metabolic origin for **1**–**3**.

Identification of the SbzP substrates

To gain further insight into the biosynthetic origin of **1**–**3**, a series of feeding experiments, utilizing the altemicidin-producing strain *S. lividans*/*sbz1* (ref. [13]) and isotopically enriched precursors, were conducted. ^{13}C-NMR and ^{1}H,^{15}N-HMBC analyses revealed significant incorporation of L-($^{13}C_4$,^{15}N)aspartic acid (fragments A and C) and ($^{13}C_3$) glycerol (fragment B) (Extended Data Fig. 1b, Supplementary Note 1). On the basis of these insights and the molecular structure of **4**, a plausible biosynthetic scenario appeared to be a SbzP-mediated [3+2]-annulation reaction between an aspartic acid-derived amino acid (fragment C) and β-nicotinamide mononucleotide (β-NMN), itself metabolically derived from aspartic acid and glyceraldehyde 3-phosphate (fragments A and B)[1].

[1]Graduate School of Pharmaceutical Sciences, The University of Tokyo, Tokyo, Japan. [2]Collaborative Research Institute for Innovative Microbiology, The University of Tokyo, Tokyo, Japan. [3]Laboratory of Molecular and Microbial Biochemistry, School of Biological Sciences, The University of Auckland, Auckland, New Zealand. [4]These authors contributed equally: Lena Barra, Takayoshi Awakawa. ✉e-mail: awakawa@mol.f.u-tokyo.ac.jp; abei@mol.f.u-tokyo.ac.jp

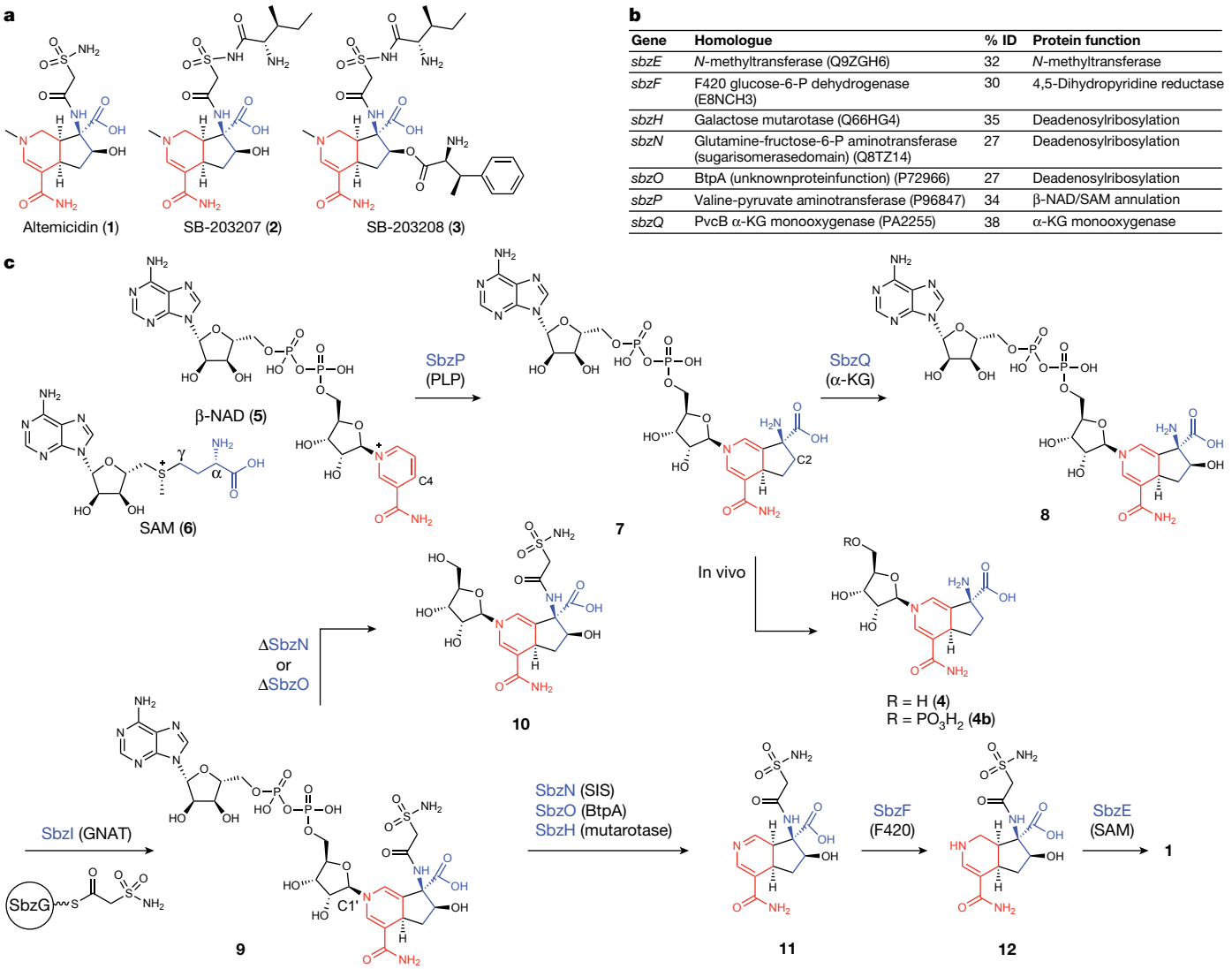

Gene	Homologue	% ID	Protein function
sbzE	*N*-methyltransferase (Q9ZGH6)	32	*N*-methyltransferase
sbzF	F420 glucose-6-P dehydrogenase (E8NCH3)	30	4,5-Dihydropyridine reductase
sbzH	Galactose mutarotase (Q66HG4)	35	Deadenosylribosylation
sbzN	Glutamine-fructose-6-P aminotransferase (sugarisomerasedomain) (Q8TZ14)	27	Deadenosylribosylation
sbzO	BtpA (unknownproteinfunction) (P72966)	27	Deadenosylribosylation
sbzP	Valine-pyruvate aminotransferase (P96847)	34	β-NAD/SAM annulation
sbzQ	PvcB α-KG monooxygenase (PA2255)	38	α-KG monooxygenase

Fig. 1 | The discovered β-NAD-utilizing *sbz* biosynthetic pathway. **a**, Structures of pathway products altemicidin (**1**), SB-203207 (**2**) and SB-203208 (**3**). **b**, A table of gene products that were functionally characterized in this study (see Supplementary Table 1 for the complete biosynthetic gene clusters). **c**, Enzymatic steps of the in vitro-reconstituted *sbz* biosynthetic pathway. % ID, percentage identity of amino acid sequences; α-KG, α-ketoglutarate-dependent dioxygenase; BtpA, BtpA protein family; F420, F420-dependent reductase; GNAT, Gcn5-related *N*-acetyltransferase; SAM, SAM-dependent methyltransferase; SIS, sugar isomerase protein.

The electrophilic *N*-ribosyl pyridinium moiety of β-NMN presumably provides sufficient reactivity towards nucleophilic addition at C4 (ref. [14]). Conversely, the corresponding alkyl nucleophile could be generated by a PLP-mediated β,γ-elimination on an α-amino acid with a Cγ-leaving group[15,16], generating a β,γ-unsaturated quinonoid (Extended Data Fig. 1b). To test this hypothesis, recombinant SbzP was incubated with β-NMN and nine candidate α-amino acid substrates, exhibiting a Cγ-leaving group (Supplementary Fig. 5). However, no detectable substrate consumption was observed. Although in vivo accumulation of **4** suggested a mononucleotide metabolic origin, we next hypothesized that dinucleotide analogues of β-NMN, namely, β-NAD (**5**) or β-nicotinamide adenine dinucleotide phosphate (β-NADP), exhibiting the same electrophilic pyridinium moiety, could be utilized by SbzP. Here, specific substrate consumption was detected for the β-NAD reaction with *S*-adenosylmethionine (SAM; **6**) (Extended Data Fig. 1c, Supplementary Fig. 6). The enzyme product was purified from preparative scale reactions and the structure was unambiguously identified as dinucleotide **7** (Fig. 1c). The finding that the SbzP expression strain accumulates **4** indicates in vivo degradation of the original dinucleotide product **7** by endogenous proteins. To further verify the function of β-NAD as the native substrate for the gatekeeping enzyme SbzP, we reconstituted the complete downstream biosynthetic pathway in vitro, guided by gene deletion experiments.

Downstream biosynthetic pathway

To gain insight into subsequent enzymatic steps in the *sbz* pathway, gene deletion strains were constructed to identify specific pathway intermediates. Deletion of *sbzE* led to accumulation of compound **12**, indicative of a terminal SAM-dependent methylation to generate **1** (Fig. 1c, Extended Data Fig. 2a). Detection of 4,5-dihydropyridine analogue **11** in the Δ*sbzF* strain suggested a penultimate imine reduction step catalysed by SbzF (Fig. 1c, Extended Data Fig. 2a). Metabolites detected in Δ*sbzN* and Δ*sbzO* cultures were identical and readily isomerized to compound **S10** during the isolation process, a cyclized derivative of the proposed original compound **10** (Fig. 1c, Supplementary Note 2). These results indicated that hydroxylation at C2 as well as sulfonamide transfer occur before deadenosylribosylation and suggested the involvement of SbzN and SbzO in the process. On the basis of the obtained insights, compound **7** was evaluated as a substrate for

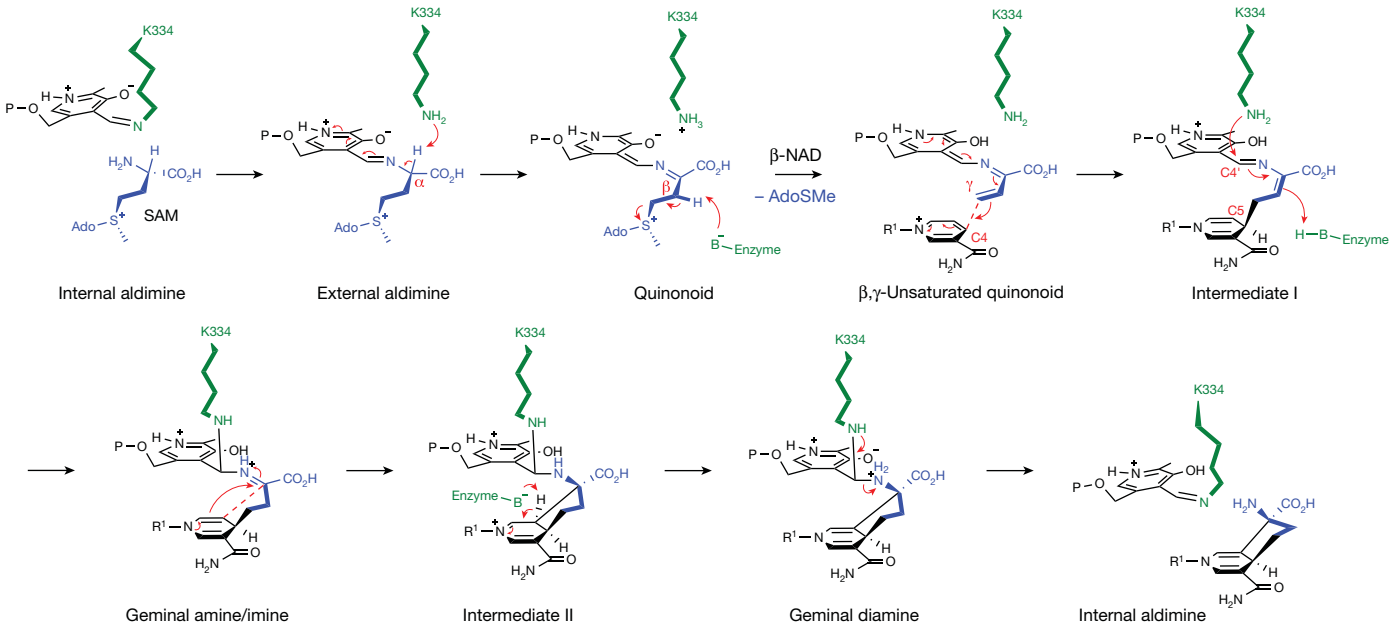

Fig. 2 | Proposed reaction mechanism of the SbzP-mediated [3+2]-annulation reaction. Relative positions of cofactors, substrates and the active site lysine residue K334 are proposed based on the typical architecture of the binding site of fold type I PLP-dependent enzymes and stereochemical considerations (Supplementary Note 7). R^1, ADP-ribose.

downstream enzymatic steps, and the results revealed that the SbzP reaction is followed by SbzQ-mediated hydroxylation at C2, yielding intermediate **8** (Fig. 1c, Extended Data Fig. 2b). Conversely, nucleoside analogue **4** was not accepted by SbzQ, indicating the importance of the ADP moiety for substrate recognition (Supplementary Fig. 10). Next, the Gcn5-related *N*-acetyltransferase enzyme SbzI, in combination with the adenylation protein SbzL and the peptidyl carrier protein SbzG[13] successfully converted **8** to **9** (Fig. 1c, Extended Data Fig. 2c). The sulfonamide transfer reaction has previously been reported to occur in the late stage of the pathway, as conversion of **S1** was demonstrated[13] (Supplementary Fig. 1). However, the conversion rate only constituted about 5%, whereas a 100% conversion of **8** to **9** was observed, indicating **8** to be the native substrate of SbzI. Incubation of SbzI + SbzG + SbzL with compound **S11**, obtained from the SbzP + SbzQ coexpression strain, led to a 10% conversion, demonstrating that similarly to SbzQ, SbzI has high substrate specificity for the β-NAD-derived dinucleotide structural motif (Supplementary Fig. 11). Compound **7** and nucleoside analogue **4** were not accepted by SbzI (Supplementary Fig. 11).

The subsequent deadenosylribosylation was successfully reconstituted by utilizing **9** as a substrate for SbzH + SbzN + SbzO, yielding **11** (Extended Data Fig. 2d, Supplementary Fig. 12). Byproducts were identified as adenosine monophosphate (AMP) and ribose 5-phosphate, indicating that removal of ADP-ribose from **9** proceeds via cleavage of the diphosphate and glycosidic bond (Extended Data Fig. 2g, Supplementary Note 1). Finally, **11** was successfully converted to **12**, utilizing the F420-dependent reductase SbzF (Fig. 1c, Extended Data Fig. 2e, Supplementary Fig. 15), and the final step in the pathway was confirmed by incubation of **12** with SbzE, resulting in the formation of altemicidin (**1**) (Extended Data Fig. 2f, Supplementary Fig. 16).

Mechanistic discussion of SbzP-mediated reaction

A proposed reaction mechanism for the SbzP-catalysed reaction is depicted in Fig. 2. The resting state of PLP enzymes typically comprises a covalent linkage of PLP to a lysine residue in the pocket of the active site (internal aldimine)[15,16]. Upon binding of SAM, an external aldimine is formed via transaldimination, and subsequent deprotonation at Cα generates a quinonoid species. Deprotonation at Cβ could then induce the elimination of 5′-methyl thioadenosine (AdoSMe), yielding a β,γ-unsaturated quinonoid, which possesses an extended conjugated π-system with a nucleophilic character at Cγ, a requisite for the proposed addition to the electrophilic C4 of β-NAD to yield intermediate I. Intermediate I comprises a dihydropyridine structural motif with a nucleophilic character at C5, and we propose addition of the active site lysine residue to C4′ of PLP to facilitate an isomerization via reprotonation at Cβ. The resulting iminium intermediate is then prone to nucleophilic addition at Cα, resulting in a second C–C bond formation event (intermediate II) and subsequent isomerization would lead to a geminal diamine species, the typical transaldimination intermediate[15–18], before release of the enzyme product and regeneration of the internal aldimine. Steady-state kinetic analyses were found to support the overall Ping-Pong Bi-Bi mechanism, in which SAM binds to the PLP-bound enzyme, releasing the first product AdoSMe while generating the transient, activated enzyme complex (β,γ-unsaturated quinonoid), which is followed by binding of β-NAD and subsequent formation of **7** (Supplementary Note 4). In line with this mechanistic model, the formation of AdoSMe was detected as a byproduct (Supplementary Fig. 21), and the formation of the β,γ-unsaturated quinonoid in the absence of β-NAD was traced by photospectroscopic investigations using a stopped-flow apparatus (Extended Data Fig. 3a, Supplementary Note 5). Furthermore, labelling experiments, utilizing ^2H_2O, and ($^2H_8$)-SAM, were in agreement with the proposed deprotonation and reprotonation steps (Supplementary Note 6). The stereochemical outcome of the reprotonation at Cβ was investigated by isolation of (*S*)-(2-^{2}H)-**7**, obtained from the SbzP reaction in ^2H_2O, indicating reprotonation of intermediate I from the *Si*-face (Supplementary Note 7). On the basis of these insights and a homology model of SbzP, a possible catalytic acid residue was identified as D139, with the single point mutation experiment leading to 85% loss in enzyme activity (Supplementary Fig. 28). The active site lysine residue, presumably responsible for covalent PLP binding, was identified as K334, based on sequence alignment to structurally characterized fold type I PLP enzymes, with the K334A point mutation leading to abolished enzyme activity (Supplementary Figs. 28, 29). Owing to higher protein stability, the SbzP homologue PsePQ (WP_185022109) was utilized for kinetic, photospectroscopic and labelling experiments. The proposed sequential C4 and C5 alkylation of β-NAD is in line with the typical reactivity of *N*-substituted pyridinium salts, which are activated

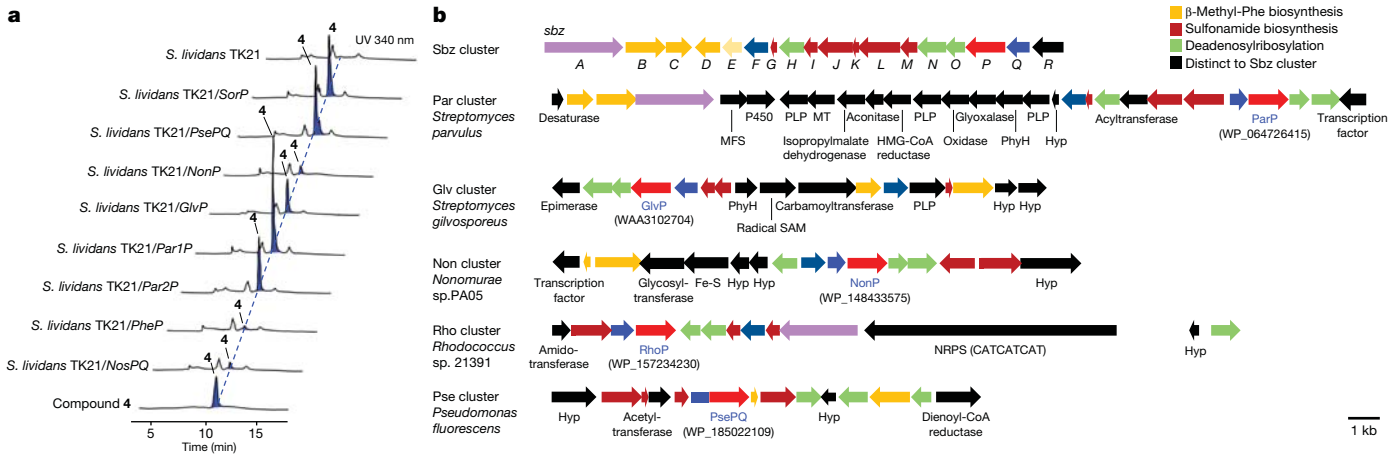

Fig. 3 | β-NAD-utilizing SbzP homologues. a, Functional characterization of representative SbzP homologues by detection of **4** in heterologous expression strains. The dashed line indicates the consistency of retention time. **b**, *sbz* cluster and selected examples of orphan biosynthetic gene clusters with SbzP homologues. *sbz* genes are grouped according to their biosynthetic function. HMG-CoA, 3-hydroxy-3-methylglutaryl-CoA; MFS, Major facilitator superfamily; MT, Methyltransferase; NRPS, Non-ribosomal peptide synthetase.

for nucleophilic addition to C4, generating reactive non-conjugated enamines (resembling intermediate I), which readily react with electrophiles to yield 3,4-dihydropyridinium species (such as intermediate II)[14]. Furthermore, a recently reported total synthesis of **1** utilized the same overall strategy of dearomative, stepwise [3+2]-cycloaddition to pyridinium salts to construct the 6-azatetrahydroindane scaffold[19]. However, an alternative mechanism, in which Cα of the β,γ-unsaturated quinonoid directly reacts with C5 of β-NAD, followed by Cγ–C4 bond formation, either stepwise or concerted, cannot be ruled out at this stage (Supplementary Fig. 30).

The SbzP enzyme family

Overall, the SbzP reaction represents the first example of a PLP-mediated tandem Cγ and Cα alkylation, ultimately leading to a [3+2]-annulation of a C4 amino acid building block to the pyridinium moiety of β-NAD. PLP-mediated Cγ alkylations have recently been reported for CndF from the citrinadin pathway and Fub7 from the fusaric acid pathway[20,21], and are proposed to proceed via a Michael addition of a carbon nucleophile to the electrophilic Cγ atom of a vinylglycine ketimine intermediate (Supplementary Fig. 32). CndF, Fub7 and mechanistically similar proteins, such as LolC[22] and Mur24 (ref. [23]) (Supplementary Fig. 33), belong to the superfamily of aspartate aminotransferase-like fold type I (AAT-I) PLP-dependent enzymes and are phylogenetically related to the cystathionine-γ-synthase-like subfamily[24] (Extended Data Fig. 3b, Supplementary Fig. 36). Conversely, PLP enzymes that catalyse Cα alkylation reactions, such as 5-aminolevulinic acid synthase[25], belong to the 2-amino-3-ketobutyrate CoA ligase subfamily (Extended Data Fig. 3b, Supplementary Fig. 36) and proceed via a quinonoid intermediate, which undergoes nucleophilic addition to an acyl-CoA ester[16,26] (Supplementary Fig. 34). SbzP also belongs to the AAT-I superfamily and exhibits the archetypical, conserved amino acid motifs, for example, involved in PLP cofactor and carboxylate binding[26] (Supplementary Fig. 29). Phylogenetically, however, SbzP and homologous proteins are evolutionary distinct to reported AAT-I subfamilies and appear on a separate branch on the phylogenetic tree (Extended Data Fig. 3b, Supplementary Fig. 36). This novel β-NAD/SAM-utilizing enzyme family is phylogenetically also not related to other SAM-utilizing PLP enzymes (Supplementary Note 8). One distinct feature of the SbzP-like family is the presence of an approximately 100 amino acid-long N-terminal domain (Supplementary Fig. 29), which was found to be essential for enzyme activity, as truncations led to completely abolished enzyme function (Supplementary Note 9).

Distribution of biosynthetic pathways utilizing β-NAD

Several members of the newly identified SbzP-like protein family were bioinformatically identified in various genomes of Gram-negative and positive bacterial phyla, such as Actinobacteria (*Streptomyces*, *Nonomuraea* and *Rhodococcus*), Chloroflexi bacteria, Proteobacteria (*Pseudomonas*, *Myxobacteria* and *Phenylobacterium*) and Cyanobacteria (*Nostoc*) (Supplementary Fig. 38). To investigate their function, eight representative examples were heterologously expressed and examination of the culture extracts of the expression strains by liquid chromatography–mass spectrometry (LC–MS) confirmed the β-NAD/SAM utilization by accumulation of nucleoside **4** for all targeted enzymes (Fig. 3a, Supplementary Table 2). Analysis of the neighbouring gene regions revealed that SbzP homologues are incorporated in various orphan biosynthetic gene clusters, distinct to the *sbz* cluster, and harbour many additional biosynthetic enzymes, such as P450 monooxygenases[27], radical SAM enzymes[28,29], non-ribosomal peptide synthetases[30], additional PLP enzymes, as well as several hypothetical proteins with so far unknown functions (Fig. 3b).

Conclusion

A novel family of gatekeeping enzymes, channelling the primary metabolites β-NAD and SAM into secondary metabolite pathways, has been identified. The obtained insights expand our understanding of the chemical biology of β-NAD and pave the way to investigate the biosynthesis of β-NAD-derived natural products.

1. Walsh, C. T. & Tang, Y. *The Chemical Biology of Human Vitamins* (RSC, 2019).
2. Cantó, C., Menzies, K. J. & Auwerx, J. NAD$^+$ metabolism and the control of energy homeostasis: a balancing act between mitochondria and the nucleus. *Cell Metab.* **22**, 31–53 (2015).
3. Depaix, A. & Kowalska, J. NAD analogs in aid of chemical biology and medicinal chemistry. *Molecules* **24**, 4187 (2019).
4. Schuller, M. et al. Molecular basis for DarT ADP-ribosylation of a DNA base. *Nature* **596**, 597–602 (2021).
5. Newman, D. J. & Cragg, G. M. Natural products as sources of new drugs over the nearly four decades from 01/1981 to 09/2019. *J. Nat. Prod.* **83**, 770–803 (2020).

6. Walsh, C. T. & Tang, Y. *Natural Product Biosynthesis: Chemical Logic and Enzymatic Machinery* (RSC, 2017).
7. Blin, K., Kim, H. U., Medema, M. H. & Weber, T. Recent development of antiSMASH and other computational approaches to mine secondary metabolite biosynthetic gene clusters. *Brief. Bioinform.* **20**, 1103–1113 (2018).
8. Houge-Frydrych, C. S. V., Gilpin, M. L., Skett, P. W. & Tyler, J. W. SB-203207 and SB-203208, two novel isoleucyl tRNA synthetase inhibitors from a *Streptomyces* sp. II. Structure determination. *J. Antibiot.* **53**, 364–372 (2000).
9. Stefanska, A. L., Cassels, R., Ready, S. J. & Warr, S. R. SB-203207 and SB-203208, two novel isoleucyl tRNA synthetase inhibitors from a *Streptomyces* sp. I. Fermentation, isolation and properties. *J. Antibiot.* **53**, 357–363 (2000).
10. Takahashi, A., Kurasawa, S., Ikeda, D., Okami, Y. & Takeuchi, T. Altemicidin, a new acaricidal and antitumor substance. I. Taxonomy, fermentation, isolation and physico-chemical and biological properties. *J. Antibiot.* **42**, 1556–1561 (1989).
11. Takahashi, A., Kurasawa, S., Ikeda, D., Okami, Y. & Takeuchi, T. Altemicidin, a new acaricidal and antitumor substance. II. Structure determination. *J. Antibiot.* **42**, 1562–1566 (1989).
12. Yan, Y., Liu, N. & Tang, Y. Recent developments in self-resistance gene directed natural product discovery. *Nat. Prod. Rep.* **37**, 879–892 (2020).
13. Hu, Z., Awakawa, T., Ma, Z. & Abe, I. Aminoacyl sulfonamide assembly in SB-203208 biosynthesis. *Nat. Commun.* **10**, 184 (2019).
14. Bull, J. A., Mousseau, J. J., Pelletier, G. & Charette, A. B. Synthesis of pyridine and dihydropyridine derivatives by regio- and stereoselective addition to n-activated pyridines. *Chem. Rev.* **112**, 2642–2713 (2012).
15. Eliot, A. C. & Kirsch, J. F. Pyridoxal phosphate enzymes: mechanistic, structural, and evolutionary considerations. *Annu. Rev. Biochem.* **73**, 383–415 (2004).
16. Du, Y. L. & Ryan, K. S. Pyridoxal phosphate-dependent reactions in the biosynthesis of natural products. *Nat. Prod. Rep.* **36**, 430–457 (2019).
17. Cook, P. D. & Holden, H. M. A structural study of GDP-4-keto-6-deoxy-D-mannose-3-dehydratase: caught in the act of geminal diamine formation. *Biochemistry* **46**, 14215–14224 (2007).
18. Hirayama, A., Miyanaga, A., Kudo, F. & Eguchi, T. Mechanism-based trapping of the quinonoid intermediate by using the K276R mutant of PLP-dependent 3-aminobenzoate synthase PctV in the biosynthesis of pactamycin. *ChemBioChem* **16**, 2484–2490 (2015).
19. Harmange Magnani, C. S. & Maimone, T. J. Dearomative synthetic entry into the altemicidin alkaloids. *J. Am. Chem. Soc.* **143**, 7935–7939 (2021).
20. Chen, M., Liu, C. T. & Tang, Y. Discovery and biocatalytic application of a PLP-dependent amino acid g-substitution enzyme that catalyzes C-C bond formation. *J. Am. Chem. Soc.* **142**, 10506–10515 (2020).
21. Hai, Y., Chen, M., Huang, A. & Tang, Y. Biosynthesis of mycotoxin fusaric acid and application of a PLP-dependent enzyme for chemoenzymatic synthesis of substituted l-pipecolic acids. *J. Am. Chem. Soc.* **142**, 19668–19677 (2020).
22. Spiering, M. J., Moon, C. D., Wilkinson, H. H. & Schardl, C. L. Gene clusters for insecticidal loline alkaloids in the grass-endophytic fungus *Neotyphodium uncinatum*. *Genetics* **169**, 1403–1414 (2005).
23. Cui, Z. et al. Pyridoxal-5′-phosphate-dependent alkyl transfer in nucleoside antibiotic biosynthesis. *Nat. Chem. Biol.* **16**, 904–911 (2020).
24. Brzovic, P. et al. Reaction mechanism of *Escherichia coli* cystathionine γ-synthase: direct evidence for a pyridoxamine derivative of vinylglyoxylate as a key intermediate in pyridoxal phosphate dependent γ-elimination and γ-replacement reactions. *Biochemistry* **29**, 442–451 (1990).
25. Bailey, H. J. et al. Human aminolevulinate synthase structure reveals a eukaryotic-specific autoinhibitory loop regulating substrate binding and product release. *Nat. Commun.* **11**, 1–12 (2020).
26. Raboni, S. et al. in *Comprehensive Natural Products II: Chemistry and Biology* Vol. 7 (eds Mander, L. & Liu, H.-W.) 273–315 (Elsevier, 2010).
27. Poulos, T. L. Heme enzyme structure and function. *Chem. Rev.* **114**, 3919–3962 (2014).
28. Ruszczycky, M. W., Zhong, A. & Liu, H. W. Following the electrons: peculiarities in the catalytic cycles of radical SAM enzymes. *Nat. Prod. Rep.* **35**, 615–621 (2018).
29. Mehta, A. P. et al. Radical *S*-adenosylmethionine (SAM) enzymes in cofactor biosynthesis: a treasure trove of complex organic radical rearrangement reactions. *J. Biol. Chem.* **290**, 3980–3986 (2015).
30. Walsh, C. T. Insights into the chemical logic and enzymatic machinery of NRPS assembly lines. *Nat. Prod. Rep.* **33**, 127–135 (2016).

Methods

General experimental procedures

Solvents and chemicals were purchased from Sigma-Aldrich, Fujifilm-Wako Pure Chemicals Ltd or Kanto Chemical Co., Inc., unless noted otherwise. Oligonucleotide primers were purchased from Eurofins Genetics. Genome data analysis and amino acid alignment were performed with MAFFT version 7 in Geneious prime version 2020.2.4(1.0). The phylogenetic trees were constructed with MUSCLE alignment and the maximum likelihood algorithm using MEGA 7.0.18. PCR was performed using a Takara PCR Thermal Cycler Dice Gradient (Takara), with Prime STAR Max DNA Polymerase (Takara). Sequence analyses were performed by Eurofins Genetics. The LC–MS analysis was performed on a Bruker Compact qTOF mass spectrometer with a Shimadzu Prominence HPLC system, using a HILIC pak VG-50 2D column (2.0 mm I.D. × 150 mm, Shodex). NMR spectra were obtained with JEOL ECX-500, JEOL ECZ-500 spectrometers, Bruker AVANCE III 900 (RIKEN Yokohama) or Bruker AVANCE III 800 (RIKEN Yokohama), and analysed with MestReNova vl0.0.2-15465. All utilized bacterial strains are summarized in Supplementary Table 3. Optical rotation values were measured by a JASCO DIP-1000 digital polarimeter. Gene deletion strains, except Δ*sbzE* and Δ*sbzO*, were constructed previously[13]. For the construction of the SbzP homology model, the I-Tasser platform was utilized[31–33].

Construction of single-gene expression strains for *sbzE*, *sbzF*, *sbzH*, *sbzN*, *sbzO*, *sbzP* or *sbzQ* in *S. lividans* TK21

The *sbzE*, *sbzF*, *sbzH*, *sbzN*, *sbzO*, *sbzP* and *sbzQ* genes were amplified from the previously constructed pZH1-*sbz1* (ref. [13]) plasmid using the primer pairs listed in Supplementary Table 3 and inserted into the pET28a vector at the HindIII and NdeI sites by in-fusion cloning (Takara), respectively. The N-Hisx6 + *sbzE*, *sbzF*, *sbzH*, *sbzN*, *sbzO*, *sbzP* and *sbzQ* genes were each amplified from the pET28 vector, using primers pET28a-pHSA81NdeIf and pET28a-pHSA81HindIIIr and inserted into the pHSA81 vector at the HindIII and NdeI sites by in-fusion cloning. The resultant pHSA81 vectors were transformed into *S. lividans* TK21 by the protoplast-PEG method. The resultant strains were named *S. lividans*/pHSA81-*sbzE*, *sbzF*, *sbzH*, *sbzN*, *sbzO*, *sbzP* and *sbzQ*.

Construction of the *sbzP* + *sbzQ* coexpression strain in *S. lividans* TK21

The *sbzP and sbzQ* genes were amplified from pZH1-*sbz1* using the primer pairs listed in Supplementary Table 3 and inserted into the pTNT vector at the *Hin*dIII and *Nde*I sites by in-fusion. The resultant vector pTNT-*sbzPQ* was transformed into *S. lividans* TK21 by the protoplast-PEG method. The obtained strain was named *S. lividans*/pTNT-*sbzPQ*.

Heterologous expression of SbzR-F in *S. lividans* TK21 for gene deletion of *sbzE*

The gene deletion construct encoding SbzR-F was divided into three parts and amplified from pZH1-*sbz1* using the primers I–VI (Supplementary Table 3). The three fragments were recombinated with the pZH1-linear fragment amplified with the primers VII–VIII (Supplementary Table 3) by in-fusion. The resulting vector was named pZH1-*sbzR-F*. Transformation of the vectors was performed by the general protoplast-PEG-mediated transformation for *S. lividans* TK21. The resultant strain was named *S. lividans*/*sbzR-F*(Δ*sbzE*).

Heterologous expression of SbzR-P and SbzN-F in *S. lividans* TK21 for gene deletion of *sbzO*

The gene cluster encoding SbzN-F was divided into two fragments and both fragments were amplified from pZH1-*sbz1* with the primers NdeI-Orf14F, primer IV, primer V and NdeI-Orf7R (Supplementary Table 3). The fragments were recombinated with the pZH2-linear fragment and amplified with the primers VII–VIII (Supplementary Table 3) by in-fusion. The resulting vector was named pZH2-*sbzN-F*. Transformation of pZH1-*sbzR-P*[13] and pZH2-*sbzN-F* was performed by the protoplast-PEG method for *S. lividans* TK21 and the obtained strain was named *S. lividans*/Δ*sbzO*.

Culture conditions for heterologous expression strains

The gene deletion strains harbouring pZH1 and/or pZH2 vectors were grown in 500-ml baffled flasks containing 100 ml Hijacking medium, consisting of 2.0% glucose, 0.3% yeast extract, 0.5% Pharma media (Archer Daniels Midland Co.), 0.3% soy broth, 2% molasses and 0.4% $CaCO_3$ (pH 7.0), for 6 days at 30 °C and 160 min^{-1}. The single-gene expression strains harbouring pHSA or pTNT were grown in 500-ml baffled flasks containing 100 ml YEME media containing 0.3% yeast extract, 0.3% malt extract, 0.5% peptone (Bacto), 1% glucose, 3.4% sucrose, 5 mM $MgCl_2$, 1% glycine (pH 7.2) and 5 μg/ml thiostrepton, for 4 days at 30 °C and 160 min^{-1}. The strain harbouring pTNT-*sbzPQ* was grown in 500-ml baffled flasks containing 100 ml YEME media with 5 μg/ml kanamycin, for 2 days at 30 °C. 5 μg/ml thiostrepton was added to the culture and further incubated for 3 days at 30 °C.

LC–MS analysis of metabolites

1.5 ml of single-gene expression or gene deletion cultures were collected and freeze dried. The residue was extracted with H_2O/MeOH (1:1), centrifuged, filtered and directly subjected to LC–MS analysis. The LC–MS solvent system was H_2O containing 50 mM NH_4HCO_2 (pH 9.0) (solvent A) and CH_3CN (solvent B) and a gradient of 100–0% B over 30 min at a flow rate of 0.2 ml/min was utilized. Mass spectra were acquired in negative-ionization mode.

Isotope feeding experiments

The altemicidin-producing strain *S. lividans*/*sbz1* was grown in 100 ml Hijacking medium and L-($^{13}C_4$, ^{15}N)aspartic acid (50 mg) or ($^{13}C_3$)glycerol (50 mg) was added to the culture after 48-h, 60-h and 72-h incubation time. The cultures were grown for 6 days and then subjected to lyophilization. Purification of altemicidin was conducted by column chromatography (Cosmosil 75C18-OPN, Nacalai Tesque, Inc.) using 50 mM ammonium acetate (pH 6.4). The fractions containing altemicidin were combined, freeze-dried and further purified by semi-preparative HPLC with a Triant C18 column (10.0 mm I.D × 250 mm, YMC), using 5% CH_3CN/H_2O as a solvent, to give 0.2 mg (($^{13}C_3$glycerol) feeding) and 0.3 mg (L-($^{13}C_4$, ^{15}N)aspartic acid feeding).

Isolation of 4 from *S. lividans*/pHSA81-SbzP

S. lividans/pHSA81-*bsbzP* was grown in 200 ml YEME medium for 5 days. Cultures were freeze-dried and extracted with water. The obtained extract was concentrated and purified by column chromatography (Sephadex LH-20 (Sigma)) using water as eluent. Target-containing fractions were pooled, concentrated and further purified by semi-preparative HPLC (HILIC Cosmosil column (10.0 mm I.D. × 250 mm, Nacalai Tesque, Inc.) and 70% CH_3CN/50 mM NH_4HCO_2 (pH 9.0)). The HPLC purification step was repeated using the same conditions and 70% CH_3CN/50 mM NH_4HCO_2 (pH 7.0) and 0.8 mg of **4** was obtained as a colourless solid. The optical rotation value of **4** was determined as $[\alpha]^{23}_{D} = +98.2$ ($c = 0.00007$, H_2O).

Isolation of S10 from *S. lividans*/Δ*sbzN* strain

S. lividans/Δ*sbzN* was grown in 200 ml Hijacking medium for 6 days. The harvested cells were freeze-dried and extracted with pure water. The obtained extract was concentrated and subjected to column chromatography, utilizing Sephadex LH-20 resin (Sigma) and water as eluent. Fractions containing **10** were pooled and further purified by semi-preparative HPLC, utilizing a HILIC Cosmosil column (10.0 mm I.D. × 250 mm) and 75% CH_3CN/50 mM NH_4HCO_2 (pH 7.4) as solvent. The obtained fraction was freeze-dried and incubated in 50 mM

NH_4HCO_2 (pH 4.0) overnight to convert **10** to **S10**. After removal of the solvent by freeze-drying, the compound was purified by HPLC with a HILIC Cosmosil column (10.0 mm I.D. × 250 mm, Nacalai Tesque, Inc), using 75% CH_3CN/50 mM NH_4HCO_2 ammonium formate (pH 5.0) as a solvent. The obtained compound was further purified under the same conditions, utilizing CH_3CN/50 mM NH_4HCO_2 (pH 9.0) as a solvent. Finally, 0.79 mg of pure **S10** was obtained as a white solid. The optical rotation value for **S10** was determined as $[\alpha]^{23}_D$ = +229.7 (c = 0.00066, H_2O).

Isolation of 12 from *S. lividans*/Δ*sbzE*

S. lividans/Δ*sbzE* was grown in 500 ml Hijacking medium for 6 days. The harvested cells were freeze-dried and extracted with pure water. The obtained extract was concentrated and subjected to column chromatography, utilizing Sephadex LH-20 resin (Sigma) and water as eluent. Fractions containing **10** were pooled and further purified by semi-preparative HPLC, utilizing a HILIC Cosmosil column (10.0 mm I.D. × 250 mm, Nacalai Tesque, Inc.) and 50% CH_3CN/50 mM ammonium formate (pH 9.0) as solvent. The compound was further purified under the same conditions using 50 mM ammonium formate (pH 7.0) as a solvent. Finally, 2.5 mg of pure **12** was obtained as a white solid. The optical rotation value of **12** was determined as $[\alpha]^{23}_D$ = −2.1 (c = 0.00023, H_2O).

Expression and purification of recombinant proteins

The *sbzE*, *sbzH*, *sbzN*, *sbzO*, *sbzQ* and *pseQ* genes on the pET28a vector were expressed in *Escherichia coli* Rosetta2 (DE3) cells by induction with 0.2 mM IPTG at 16 °C. The *sbzF* gene was expressed in *E. coli* LOBSTR (kerafast) harbouring pBB528 and pBB541 (addgene), by induction with 0.7 mM IPTG at 14 °C. SbzP was expressed and purified from *S. lividans*/pHSA81 transformant.

For protein purifications (except SbzF) the pellets were resuspended in buffer A (50 mM HEPES, pH 8.0, 300 mM NaCl) + 5 mM imidazole and lysed by sonication on ice. Cellular debris was removed by centrifugation (13,000*g*, 15 min, 4 °C). The supernatant was loaded onto Ni-NTA agarose resin (Fujifilm-Wako) in a gravity flow column, which was washed with buffer A + 20 mM imidazole followed by elution with buffer A + 500 mM imidazole. The purified proteins were concentrated using Amicon Ultra filters, and buffer exchanged into buffer A, using PD-10 desalting column (GE Healthcare). The purified proteins were flash-frozen in liquid nitrogen and stored at −80 °C. The proteins SbzG, SbzI and SbzL were prepared as described before[13].

For the purification of SbzF, the pellets were resuspended in buffer B (50 mM HEPES pH 7.8, 500 mM NaCl, 5 mM β-mercaptoethanol, 13% glycerol) + 10 mM imidazole and lysed by sonication on ice. Cellular debris was removed by centrifugation (13,000*g*, 15 min, 4 °C). The supernatant was loaded onto Ni-NTA agarose resin (Fujifilm-Wako) in a gravity flow column, which was washed with buffer B + 10 mM imidazole followed by elution with buffer B + 500 mM imidazole. The protein was further purified to homogeneity by gel-filtration chromatography on a HiLoad 16/60 Superdex 200-pg column (GE Healthcare) with buffer C (25 mM HEPES pH 7.8, 500 mM NaCl, 0.1 mM tris(2-carboxyethyl) phosphine, 10% glycerol). The purified proteins were flash-frozen in liquid nitrogen and stored at −80 °C.

Isolation of 7 from the large-scale SbzP reaction

The enzyme reaction was performed in 70 × 500-µl portions, each utilizing 1 mM SAM, 1 mM β-NAD, 0.2 mM PLP and 10 µM SbzP in 50 mM potassium phosphate buffer (pH 8.0) at 30 °C for 18 h. The reactions were pooled, freeze-dried and subjected to column chromatography (Sephadex LH-20, sigma) with water at 4 °C. Fractions containing **7** were combined, concentrated and further purified by semi-preparative HPLC (HILIC Cosmosil column, 10.0 mm I.D. × 250 mm), using 50% CH_3CN/50 mM NH_4HCO_2 (pH 9.0) as solvent). 1.20 mg of **7** was obtained as a colourless solid. The optical rotation value of **7** was determined as $[\alpha]^{23}_D$ = +18.0 (c = 0.00014, H_2O).

Isolation of 8 from the large-scale PsePQ reaction

The enzyme reaction was performed on 70 × 500-µl scale, consisting of 1 mM SAM, 1 mM NAD^+, 0.2 mM PLP and 22.1 µM PsePQ in 50 mM HEPES (pH 8.0) buffer at 30 °C for 1 h. Subsequently, 2.5 mM α-ketoglutaric acid, 2.0 mM L-ascorbate, 0.1 mM $FeSO_4$ and 13.5 µM PseQ were added and incubated at 30 °C for 2 h. The reaction was freeze-dried and subjected to column chromatography (Sephadex LH-20, eluent: water) at 4 °C and fractions containing **8** were combined and further purified by semi-preparative HPLC with HILIC Cosmosil column (10.0 mm I.D. × 250 mm), using 50% CH_3CN/50 mM NH_4HCO_2 (pH 9.0) as the solvent. Finally, 0.76 mg of **8** was obtained as a white powder. The optical rotation value of **8** was determined as $[\alpha]^{23}_D$ = −71.2 (c = 0.00063, H_2O).

Preparation of 9 from the large-scale SbzI + SbzG + SbzL enzyme reaction

The enzyme reaction was performed on 35 × 500-µl scale, consisting of 0.5 mM **8**, 1 mM $MgCl_2$, 1 mM DTT, 0.2 mM ATP, 1 mM sulfamoylacetic acid, 10 µM SbzI, 250 µM SbzG and 10 µM SbzL in 50 mM potassium phosphate buffer (pH 8.0) at 30 °C for 6 h. The reactions were pooled, freeze-dried and subjected to column chromatography (Sephadex LH-20, eluent: water) at 4 °C. Fractions containing **9** were combined, concentrated and directly used for in vitro reactions. The concentration was estimated, based on the observed complete conversion of **8**.

Preparation of 11 from *S. lividans*/Δ*sbzF* strain

S. lividans/Δ*sbzF* was incubated in 2 l Hijacking medium containing 0.3% yeast extract, 0.2% pharma media, 0.3% soy broth, 2.0% glucose, 2.0% molasses and 0.4% $CaCO_3$ (pH 7.0) at 30 °C for 6 days. The culture broth was freeze-dried and subjected to column chromatography, utilizing activated charcoal with water. Fractions containing **11** were freeze-dried and further purified by Sephadex LH-20 (Sigma) with 10% $(CH_3)_2CO/H_2O$ as a solvent. The fractions containing **11** were combined, freeze-dried and used for in vitro reactions.

Heterologous expression of SbzP + SbzQ in *S. lividans* TK21 and isolation of S11

S. lividans/pTNT-SbzPQ was grown in 1.5 l YEME medium for 5 days. Cultures were freeze-dried, extracted with pure water and treated with BAP (Takara) for 1 h in 37 °C. The water-soluble fraction was purified by Sephadex LH-20 with water as eluent. The fractions containing **S11** were further purified by semi-preparative HPLC with HILIC Cosmosil column (10.0 mm I.D. × 250 mm) three times, using 75% CH_3CN/50 mM NH_4HCO_2 at different pH (9.0 → 7.4 → 9.0). Finally, 0.89 mg of **S11** was obtained as a white powder. The optical rotation value of **S11** was determined as $[\alpha]^{22}_D$ = +106.2 (c = 0.00074, H_2O).

Enzyme assay of SbzP

The reaction mixture (50 µl) contained 1 mM β-NAD, 1 mM SAM, 0.1 mM PLP and 10 µM SbzP in 50 mM HEPES (pH 8.0) buffer and was incubated at 30 °C overnight. The reaction was quenched by addition of 50 µl methanol and the precipitated protein was removed by centrifugation. The supernatant was subjected to LC–MS analysis (solvent A: 50 mM NH_4HCO_2 (pH 9.0), solvent B: CH_3OH, solvent gradient: 100–0% B over 30 min at a flow rate of 0.2 ml/min, negative-ionization mode).

Enzyme assay of SbzQ

The reaction mixture (50 µl) contained 0.5 mM **7**, 5 mM α-ketoglutarate, 4 mM L-ascorbic acid, 0.2 mM $FeSO_4$ and 10 µM SbzQ in 50 mM HEPES (pH 7.4) buffer and was incubated at 30 °C for 1 h. The reaction was quenched by addition of 50 µl methanol and the precipitated protein was removed by centrifugation. The supernatant was subjected to LC–MS analysis (solvent A: 50 mM NH_4HCO_2 (pH 9.0), solvent B: CH_3OH, solvent gradient: 100–0% B over 30 min at a flow rate of 0.2 ml/min, negative-ionization mode).

Enzyme assay of SbzI + SbzG + SbzL

The reaction mixture (50 µl) contained 0.5 mM **8**, 1 mM $MgCl_2$, 1 mM DTT, 0.2 mM ATP, 1 mM sulfamoylacetic acid, 10 µM SbzI, 250 µM SbzG and 10 µM SbzL in 50 mM HEPES buffer (pH 8.0) at 30 °C for 6 h. The reaction was quenched by addition of 50 µl methanol and the precipitated protein was removed by centrifugation. The supernatant was subjected to LC–MS analysis (solvent A: 50 mM NH_4HCO_2 (pH 9.0), solvent B: CH_3OH, solvent gradient: 100–0% B over 40 min at a flow rate of 0.2 ml/min, negative-ionization mode).

Enzyme assay of SbzN + SbzO + SbzH

The reaction mixture (50 µl) contained 0.5 mM **9**, 10 µM SbzN, 10 µM SbzO and 10 µM SbzH in 50 mM HEPES buffer (pH 8.0) at 30 °C for 2 h. The reaction was quenched by addition of 50 µl methanol and the precipitated protein was removed by centrifugation. The supernatant was subjected to LC–MS analysis (solvent A: 50 mM NH_4HCO_2 (pH 9.0), solvent B: CH_3OH, solvent gradient: 100–0% B over 30 min at a flow rate of 0.2 ml/min, negative-ionization mode).

Enzyme assay of SbzF

The reaction mixture (50 µl) contained 15 µl of crude **11** (prepared as described above), 1 mM glucose-6-phosphate, 10 µM SbzF, 50 µM glucose-6-phosphate dehydrogenase FGD and 0.1 mM F420 in 50 mM HEPES buffer (pH 7.8) at 30 °C for 1 h (refs. [34–36]). The reaction was quenched by addition of 50 µl methanol and the precipitated protein was removed by centrifugation. The supernatant was subjected to LC–MS analysis (solvent A: 50 mM NH_4HCO_2 (pH 9.0), solvent B: CH_3OH, solvent gradient: 100–0% B over 30 min at a flow rate of 0.2 ml/min, negative-ionization mode).

Enzyme assay of SbzE

The reaction mixture (50 µl) contained 0.5 mM **12**, 1 mM SAM and 10 µM SbzE in 50 mM HEPES buffer (pH 8.0) at 30 °C for 2 h. The reaction was quenched by addition of 50 µl methanol and the precipitated protein was removed by centrifugation. The supernatant was subjected to LC–MS analysis (solvent A: 50 mM NH_4HCO_2 (pH 9.0), solvent B: CH_3OH, solvent gradient: 100–0% B over 30 min at a flow rate of 0.2 ml/min, negative-ionization mode).

Cloning and expression of SbzP homologues

The *par1P*, *par2P*, *glvP*, *nonP* and *sorP* genes were amplified from gDNA of *Streptomyces parvulus* NBRC 13193, *Streptomyces gilvosporeus*, *Nonomuraea jiangxiensis* or *Sorangium cellulosum* So Ce56 using the primer pairs listed in Supplementary Table 3 and inserted into the pQTev vector at the HindIII and BamHI sites. The *nosPQ*, *pheP*, *pseQ* and *psePQ* genes were amplified from synthetic genes purchased from Fasmac (Supplementary Data) and inserted into the pQTev vector at the HindIII and BamHI sites. The N-Hisx6 + *sbzP* was amplified from pET28-*sbzQ* by using primers pET28a-pHSA81NdeIf & pET28a-pHSA81HindIIIr, and the N-Hisx7 + *par1P*, *par2P*, *sorP*, *nonP*, *glvP*, *nosPQ*, *pheP*, clxP, *rhoP* and *psePQ* genes were further amplified from each of the pQTev expression vector by using primers pQTev-pHSA81NdeIf and pQTev-pHSA81HindIIIr. Each PCR fragment was inserted into the pHSA81 vector at the HindIII and NdeI sites by in-fusion. As described above, the strains were grown in 500-ml baffled flasks containing 100 ml YEME media with 5 µg/ml thiostrepton. Produced metabolites were analysed as described above.

Cloning and expression of SbzP variants

For, SbzP_K334A, the *N-sbzP*K334A and *C-sbzP*K334A were amplified by using the primers with pQTevSbzP_F & SbzPK334A_R, and SbzPK334A_F & pQTevSbzP_R, respectively. The two fragments were recombinated and inserted into the pQTev vector at the *Hin*dIII and *Bam*HI sites by in-fusion, to give pQTev-*sbzP*K334A. *Nhis-sbzP*K334A was further amplified from pQTev-*sbzP*K334A, ligated into pHSA81 and expressed in *S. lividans* as described above. For PsePQ_D435N, the quikchange method with primers PsePQ_D435N_f & PsePQ_D435N_r was used on pQTev-PsePQ, and the mutated *psePQ* was inserted into pHSA81. SbzP N-terminal truncates (9S, 10P, 11R, 17Q, 25R, 33R, 38P, 47L and 60L) were amplified with pQTev-SbzP-X-BamHIf & pQTevSbzP_R, and inserted into pHSA81 via pQTev. The protein expression was carried out in *S. lividans* TK21 as described above.

Enzyme assay of SbzP and PsePQ variants

Nhis SbzP wild type and variants were purified as described for SbzP. 5 µM of the enzyme was incubated with 0.1 mM PLP, 1.0 mM SAM and 1.0 mM β-NAD at 28 °C in 2 h in 50 mM potassium phosphate (pH 7.8). The quench and analysis were done as described as the same way as the SbzP reaction.

Inhibitor assay with S2-S9 and AdoSMe

4.4 µM of PsePQ was incubated with 0.1 mM PLP, 1.0 mM SAM and 1.0 mM β-NAD, in the presence of 1.0 mM **S2**-**S9** and AdoSMe at 28 °C in 2 h in 50 mM potassium phosphate (pH 7.8). Reaction rates were measured spectrophotometrically (Infinite 200 PRO) by monitoring the formation of enzyme product **7** at λ = 338 nm.

Isotopic labelling experiments with ($^2H_8$)-SAM and ^2H_2O

($^2H_8$)-SAM was enzymatically synthesized from L-($^2H_8$)methionine (Cambridge Isotope Laboratories) and ATP, as reported[37]. The SbzP homologue PsePQ was utilized for all assays and purified as described for SbzP above. For the reaction in ^2H_2O, recombinant enzyme was buffer-exchanged to potassium phosphate buffer (50 mM, pH 8.0, 300 mM NaCl in ^2H_2O) by usage of PD-10 desalting columns (Cytiva) and the concentration was adjusted to 20 µM. Analytical enzyme reactions (100 µl) contained 20 µM enzyme, 0.1 mM PLP, 1 mM β-NAD, and 1 mM SAM or 1 mM ($^2H_8$)-SAM. Reactions were carried out at 30 °C for 2 h and then analysed by LC–MS as described above. For the conversion of the obtained isotopologues of **7** to **8**, the reactions were repeated and after 2 h, 5 mM α-ketoglutarate, 4 mM L-ascorbic acid and 0.2 mM $FeSO_4$ were added and incubated for another 1 h at 30 °C, followed by LC–MS analysis as described above. For the preparative isolation of (*S*)-(2-^{2}H)-**7**, 35 × 200-µl enzyme reactions were conducted, utilizing PsePQ as described for the analytical reactions above. The reactions were pooled, freeze-dried and subjected to column chromatography (Sephadex LH-20) with water at 4 °C. Fractions containing (*S*)-(2-^{2}H)-**7** were combined, concentrated and further purified by semi-preparative HPLC (HILIC Cosmosil column, 10.0 mm I.D. × 250 mm), using 50 % CH_3CN/50 mM NH_4HCO_2 (pH 9.0) as solvent). 0.50 mg of (*S*)-(2-^{2}H)-**7** were obtained as a colourless solid and analysed by ^{1}H-NMR (Supplementary Fig. 25).

Photospectroscopic investigations

The SbzP homologue PsePQ was utilized and purified by Ni-NTA affinity chromatography with buffer containing 50 mM potassium phosphate (pH 7.8), 300 mM NaCl and 100 µM PLP, as described above. Free PLP was removed by PD-10 desalting columns, using 50 mM potassium phosphate (pH 7.8, 300 mM NaCl). For the stopped-flow analysis (SX. 18MV-R; Applied Photophysics), the protein was utilized at a concentration of 20 µM. UV absorption between λ = 300 and 600 nm was recorded at 4 °C for (1) PsePQ, (2) PsePQ after addition of 5 mM of SAM, and (3) SbzP after addition of 5 mM of SAM and β-NAD. For the UV spectral analysis described in Supplementary Fig. 23, the enzyme was purified by Ni-NTA affinity chromatography in the same way as the stopped-flow experiment, and further purified by gel-filtration chromatography on a HiLoad 16/60 Superdex 200 pg column (Cytiva) with buffer containing 50 mM potassium phosphate (pH 7.8) and 300 mM NaCl. 27 µM of enzyme was mixed with 5 mM SAM and 5 mM β-NAD in a stepwise manner (Supplementary Fig. 23c) or mixed with the 5 mM solution consisting of 5 mM SAM and 5 mM β-NAD (Supplementary

Fig. 23d). All spectra were measured with Cary 60 UV-Vis spectrophotometer (Agilent Technologies).

Kinetic analysis

The PsePQ enzyme for kinetic analysis was purified by Ni-NTA affinity chromatography in the same way as photospectroscopic investigations, and further purified by gel-filtration chromatography on a HiLoad 16/60 Superdex 200-pg column (Cytiva) with buffer containing 50 mM potassium phosphate (pH 7.8), 300 mM NaCl, 100 μM PLP and 5% glycerol. The purified proteins were flash-frozen in liquid nitrogen and stored at −80 °C. Reaction rates were measured spectrophotometrically (Infinite 200 PRO) by monitoring formation of enzyme product **7** at λ = 338 nm. All measurements were performed in triplicate at 28 °C. The reactions were started by addition of 4.4 μM PsePQ, was incubated for 10 min for variable β-NAD (20–200 μM) and fixed SAM (400, 700 and 1,000 μM) concentrations, and for 20 min for variable SAM (20–200 μM) and fixed β-NAD (500, 800 and 1,000 μM) concentrations (Supplementary Note 4). Initial velocity (Y) and variable substrate concentration (X) were plotted, and kinetic parameters were calculated by fitting the data to the equation $Y = V_{max} \times X/(K_m + X)$ in GraphPad Prism 9.0. For inhibition assays, 4.4 μM of PsePQ was incubated with 0, 200 or 400 μM of AdoSMe in combination with variable concentrations of β-NAD (20–1,000 μM), but fixed SAM concentration (1,000 μM), and with 0, 100 or 200 μM of β-NADH and variable SAM (10–1,000 μM) and fixed β-NAD concentration (1,000 μM). The absorption of β-NADH in each reaction was subtracted from the total absorption at λ = 338 nm.

Data availability

Data that support the findings of this study are available within the paper and its Supplementary Information, or are available from the corresponding authors upon request.

31. Zhang, Y. I-TASSER server for protein 3D structure prediction. *BMC Bioinformatics* **9**, 1–8 (2008).
32. Roy, A., Kucukural, A. & Zhang, Y. I-TASSER: a unified platform for automated protein structure and function prediction. *Nat. Protoc.* **5**, 725–738 (2010).
33. Roy, A., Yang, J. & Zhang, Y. COFACTOR: an accurate comparative algorithm for structure-based protein function annotation. *Nucleic Acids Res.* **40**, 471–477 (2012).
34. Bashiri, G., Rehan, A. M., Greenwood, D. R., Dickson, J. M. J. & Baker, E. N. Metabolic engineering of cofactor F420 production in *Mycobacterium smegmatis*. *PLoS ONE* **5**, 1–10 (2010).
35. Bashiri, G., Squire, C. J., Baker, E. N. & Moreland, N. J. Expression, purification and crystallization of native and selenomethionine labeled *Mycobacterium tuberculosis* FGD1 (Rv0407) using a *Mycobacterium smegmatis* expression system. *Protein Expr. Purif.* **54**, 38–44 (2007).
36. Oyugi, M. A., Bashiri, G., Baker, E. N. & Johnson-winters, K. Investigating the reaction mechanism of F 420-dependent glucose-6-phosphate dehydrogenase from *Mycobacterium tuberculosis*: kinetic analysis of the wild-type and mutant enzymes. *Biochemistry* **55**, 5566–5577 (2016).
37. McCarty, R. M., Krebs, C. & Bandarian, V. Spectroscopic, steady-state kinetic, and mechanistic characterization of the radical SAM enzyme QueE, which catalyzes a complex cyclization reaction in the biosynthesis of 7-deazapurines. *Biochemistry* **52**, 188–198 (2013).

Acknowledgements This work was supported by a Grant-in-Aid for Scientific Research from the Ministry of Education, Culture, Sports, Science and Technology, Japan (JSPS KAKENHI grant numbers JP16H06443, JP17H04763, JP19H04641, JP20H00490, JP20KK0173 and JP21K18246), the New Energy and Industrial Technology Development Organization (NEDO, Grant Number JPNP20011) and AMED (Grant Number JP21ak0101164), Japan Science and Technology Agency (JST SICORP grant number JPMJSC1701), UTEC-UTokyo FSI Research Grant Program, Mochida Memorial Foundation for Medical and Pharmaceutical Research, and Takeda Science Foundation, Kato Memorial Bioscience Foundation, The Asahi Glass Foundation, and a Sir Charles Hercus Fellowship (Health Research Council of New Zealand) to G.B. (17/058). We thank GlaxoSmithKline for providing *Streptomyces* sp. NCIMB 40513; G. Cao for providing *S. gilvosporeus* F607; M. Kobayashi for providing pHSA81; Deutsche Forschungsgemeinschaft (DFG BA 6870/1-1) for a postdoctoral research fellowship to L.B.; T. Mori and R. Ushimaru for critical reading of the manuscript; F. Kudo, T. Eguchi and T. Ueda for instruction on the stopped flow apparatus; and H. Zhang, F. Hayashi and Y. Ishii for measurement of NMR spectra at RIKEN Yokohama.

Author contributions T.A. and I.A. conceived the idea for the study. L.B., T.A. and I.A. developed the hypothesis and designed the experiments. L.B. and T.A. performed the in vivo and in vitro experiments. L.B. and K.S. performed compound isolation and characterization. L.B. and T.A. performed bioinformatic analysis to identify biosynthetic gene clusters and protein functions. L.B., T.A. and K.S. performed protein purification. G.B. expressed SbzF and provided the F420 cofactor regeneration system. T.A. and Z.H. performed the feeding experiments. All authors analysed and discussed the results. L.B., T.A. and I.A. prepared the manuscript.

Competing interests The authors declare no competing interests.

Correspondence and requests for materials should be addressed to Takayoshi Awakawa or Ikuro Abe.

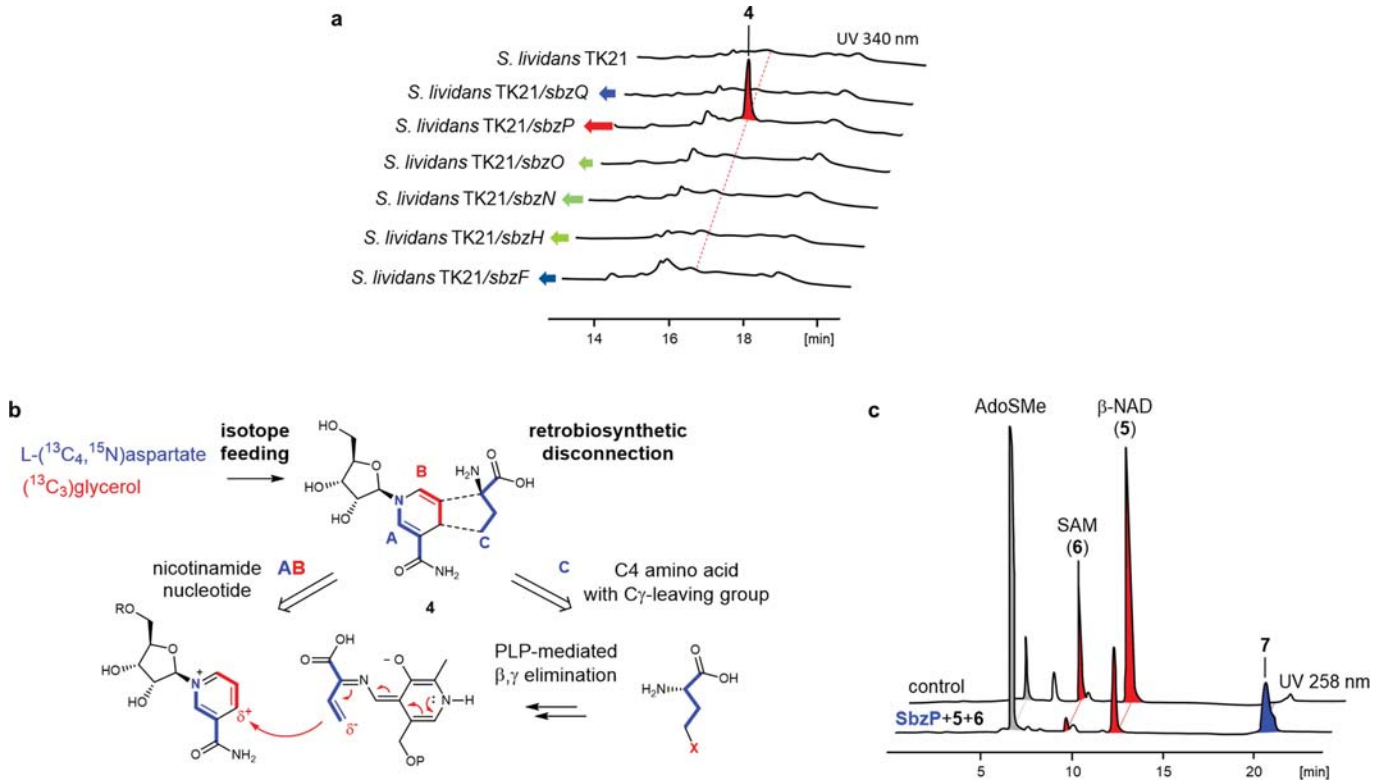

Extended Data Fig. 1 | Identification of the gatekeeping enzyme SbzP. **a**, LC-MS analysis of single gene expression culture extracts (UV trace 340 nm). **b**, Summary of isotope feeding experiment results and retrobiosynthetic considerations. **c**, LC-MS analysis of the productive SbzP substrate combination of β-NAD (**5**) and SAM (**6**) with concomitant appearance of dinucleotide product **7** (UV trace 258 nm). "Control" indicates incubation of substrates without enzyme.

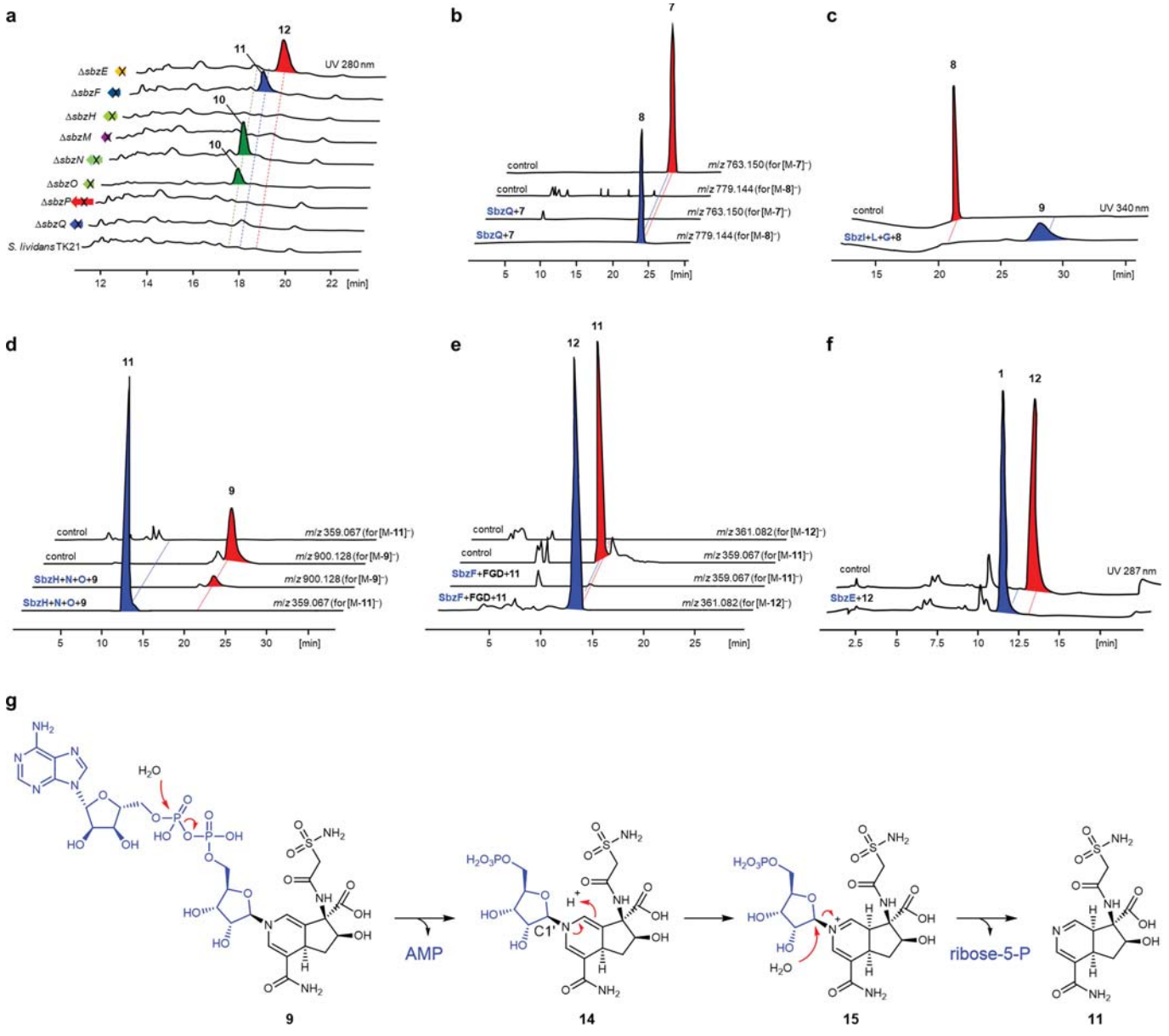

Extended Data Fig. 2 | Gene deletion-guided *in vitro* reconstitution of the *sbz* pathway. a, LC-MS analysis of gene deletion strain culture extracts (UV trace 280 nm). **b**, LC-MS analysis of SbzQ-mediated conversion of **7** to **8** (EIC traces of substrate and product). **c**, LC-MS analysis of SbzI reaction of **8** to **9** (UV trace 340 nm). **d**, LC-MS analysis of deadenosylribosylation catalyzed by SbzN+O+H (EIC traces of substrate and product). **e**, LC-MS analysis of F_{420}-dependent reduction of **11** to **12** (EIC traces of substrate and products). **f**, LC-MS analysis of SbzE-mediated methylation towards **1** (UV trace 287 nm). **g**, Proposed steps in the deadenosylribosylation reaction. "Control" indicates incubation of substrates without enzyme(s).

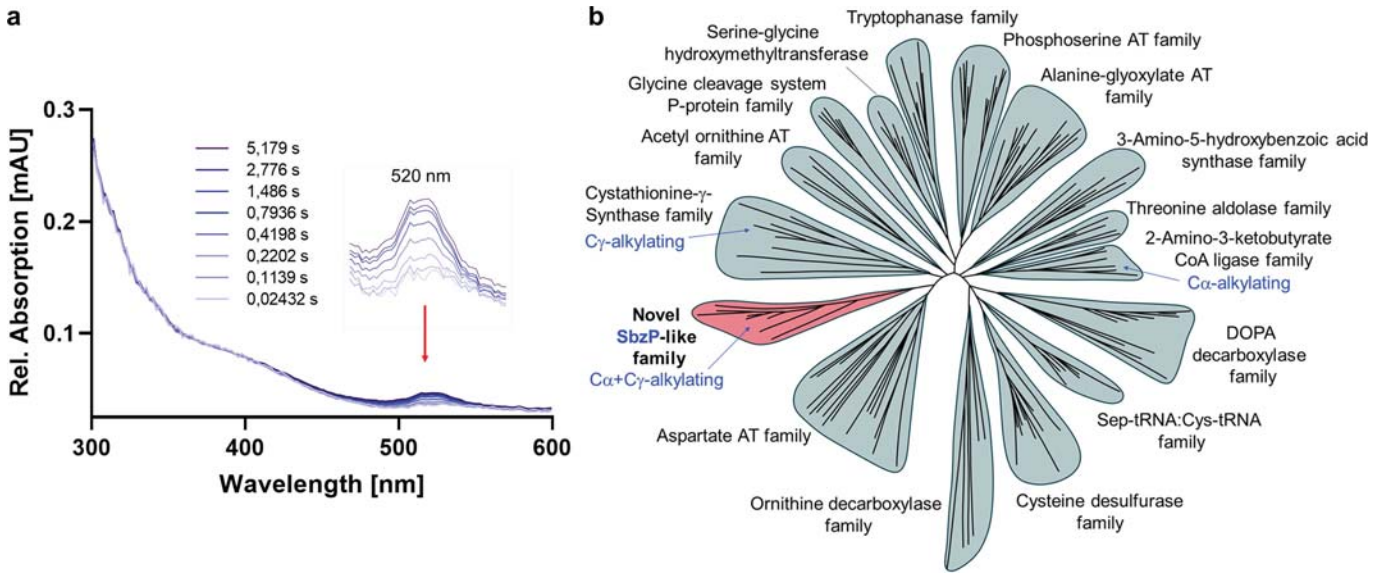

Extended Data Fig. 3 | SbzP as a functionally and phylogenetically distinct PLP-dependent enzyme family. a, Time-resolved photospectroscopic changes of SbzP after addition of SAM (**6**) (see Supplementary Note 5 for further details). **b**, Phylogenetic analysis of SbzP and reported subfamily members of the AAT-I protein superfamily.